

High precision wavelength estimation method for integrated optics

R. M. Oldenbeuving,^{1,2,3} H. Song,^{4,5,6,*} G. Schitter,⁷ M. Verhaegen,⁵
E. J. Klein,⁸ C. J. Lee,^{1,2,9} H. L. Offerhaus^{2,10} and K.-J. Boller^{1,2}

¹University of Twente, Laser Physics and Nonlinear Optics Group, PO Box 217, 7500 AE, Enschede, The Netherlands

²MESA+ Research Institute for Nanotechnology, PO Box 217, 7500 AE, Enschede, The Netherlands

³Satrax B.V., PO Box 456, 7500 AL, Enschede, The Netherlands

⁴State Key Lab of Modern Optical Instrumentation, Zhejiang University, 310027, Hangzhou, China

⁵Delft Center for Systems and Control, Delft University of Technology, Mekelweg 2, 2628 CD, Delft, The Netherlands

⁶Ocean College, Zhejiang University, Yuhangtang Road 866, 310058, Hangzhou, China

⁷Automation and Control Institute, Vienna University of Technology, Gusshausstrasse 27-29, A-1040, Vienna, Austria

⁸XiO Photonics, PO Box 1254, 7500 BG, Enschede, The Netherlands

⁹FOM Institute DIFFER, Edisonbaan 14, 3439 MN, Nieuwegein, The Netherlands

¹⁰University of Twente, Optical Sciences Group, PO Box 217, 7500 AE, Enschede, The Netherlands

*hongsong@zju.edu.cn

Abstract: A novel and simple approach to optical wavelength measurement is presented in this paper. The working principle is demonstrated using a tunable waveguide micro ring resonator and single photodiode. The initial calibration is done with a set of known wavelengths and resonator tunings. The combined spectral sensitivity function of the resonator and photodiode at each tuning voltage was modeled by a neural network. For determining the unknown wavelengths, the resonator was tuned with a set of heating voltages and the corresponding photodiode signals were collected. The unknown wavelength was estimated, based on the collected photodiode signals, the calibrated neural networks, and an optimization algorithm. The wavelength estimate method provides a high spectral precision of about 8 pm ($5 \cdot 10^{-6}$ at 1550 nm) in the wavelength range between 1549 nm to 1553 nm. A higher precision of 5 pm ($3 \cdot 10^{-6}$) is achieved in the range between 1550.3 nm to 1550.8 nm, which is a factor of five improved compared to a simple lookup of data. The importance of our approach is that it strongly simplifies the optical system and enables optical integration. The approach is also of general importance, because it may be applicable to all wavelength monitoring devices which show an adjustable wavelength response.

© 2013 Optical Society of America

OCIS codes: (120.4140) Monochromators; (120.6200) Spectrometers and spectroscopic instrumentation; (130.3120) Integrated optics devices; (140.4780) Optical resonators.

References and links

1. X. J. Gu, "Wavelength-division multiplexing isolation fiber filter and light source using cascaded long-period fiber gratings," *Opt. Lett.* **23**(7), 509–510 (1998).

2. N. Ophir, R. K. W. Lau, M. Menard, X. Zhu, K. Padmaraju, Y. Okawachi, R. Salem, M. Lipson, A. L. Gaeta, and K. Bergman, "Wavelength conversion and unicast of 10-Gb/s data spanning up to 700 nm using a silicon nanowaveguide," *Opt. Express* **20**(6), 6488–6495 (2012).
3. G. Wysocki, R. F. Curl, F. K. Tittel, R. Maulini, J. M. Bulliard, and J. Faist, "Widely tunable mode-hop free external cavity quantum cascade laser for high resolution spectroscopic applications," *Appl. Phys. B-Lasers O.* **81**(6), 769–777 (2005).
4. I. Lindsay, B. Adhimoalam, P. Gross, M. Klein, and K. Boller, "110GHz rapid, continuous tuning from an optical parametric oscillator pumped by a fiber-amplified DBR diode laser," *Opt. Express* **13**(4), 1234–1239 (2005).
5. J. B. Cooper, P. E. Flecher, S. Albin, T. M. Vess, and W. T. Welch, "Elimination of mode hopping and frequency hysteresis in diode laser raman spectroscopy: the advantages of a distributed bragg reflector diode laser for raman excitation," *Appl. Spectrosc.* **49**, 1692–1698 (1995).
6. K. Richard, P. Manson, and P. Ewart, "A widely tunable, high power, single-mode laser for linear and nonlinear spectroscopy," *Meas. Sci. Tech.* **19**, 015603 (2008).
7. T. Udem, R. Holzwarth, and T. W. Hänsch, "Optical frequency metrology," *Nature* **416**(6877), 233–237 (2002).
8. A. Banerjee, U. D. Rapol, A. Wasan, and V. Natarajan, "High-accuracy wavemeter based on a stabilized diode laser," *Appl. Phys. Lett.* **79**, 2139–2141 (2001).
9. Q. Wang, G. Farrell, T. Freir, G. Rajan, and P. Wang, "Low-cost wavelength measurement based on a macrobending single-mode fiber," *Opt. Lett.* **31**(12), 1785–1787 (2006).
10. P. Kiesel, O. Schmidt, S. Mohta, N. Johnson, and S. Malzer, "Compact, low-cost, and high-resolution interrogation unit for optical sensors," *Appl. Phys. Lett.* **89**, 201113 (2006).
11. E. Viasnoff-Schwoob, C. Weisbuch, H. Benisty, C. Cuisin, E. Derouin, O. Drisse, G-H Duan, L. Legouézigou, O. Legouézigou, F. Pommereau, S. Golka, H. Heidrich, H. J. Hensel, and K. Janiak, "Compact wavelength monitoring by lateral outcoupling in wedged photonic crystal multimode waveguides," *Appl. Phys. Lett.* **86**, 101107 (2005).
12. C. Sookdhis, T. Mei, H. S. Djie, and J. Arokiaraj, "Passive wavelength monitor based on multimode interference waveguide," *Opt. Eng.* **42**(12), 3421–3422 (2003).
13. B. Mason, S. P. DenBaars, and L. A. Coldren, "Tunable sampled-grating DBR lasers with integrated wavelength monitors," *IEEE Photonic. Tech. L.* **10**(8), 1085–1087 (1998).
14. F. Morichetti, A. Melloni, M. Martinelli, R. G. Heideman, A. Leinse, D. H. Geuzebroek, and A. Borreman, "Box shaped dielectric waveguides: A new concept in integrated optics," *J. Lightwave Technol.* **25**, 2579–2589 (2007).
15. J. F. de Boer, M. P. van Albada, and A. Lagendijk, "Transmission and intensity correlations in wave propagation through random media," *Phys. Rev. B* **45**, 658–666 (1992).
16. B. Redding and H. Cao, "Using a multimode fiber as a high-resolution, low-loss spectrometer," *Opt. Lett.* **37**(16), 3384–3386 (2012).
17. J. Sjöberg, Q. Zhang, L. Ljung, A. Benveniste, B. Delyon, P. Glorennec, H. Hjalmarsson, and A. Juditsky, "Non-linear black-box modeling in system identification: a unified overview," *Automatica* **31**(12), 1691–1724 (1995).
18. R. Lippmann, "An introduction to computing with neural nets," *IEEE ASSP Magazine* **4**(2), 4–22 (1987).
19. S. Y. Kung, *Digital Neural Networks*. (Prentice-Hall, 1993).
20. S. Haykin, *Neural Networks: a Comprehensive Foundation*. (Macmillan, 1994).
21. H. Demuth, M. Beale, and M. Hagan, *MATLAB Neural Network Toolbox 5 User's Guide*. (The MathWorks, Inc., 2007).
22. M. Verhaegen and V. Verdult, *Filtering and System Identification: A Least Squares Approach*. (Cambridge University, 2007).

1. Introduction

Measuring and controlling the wavelength of lasers is essential to a vast number of applications. Examples range from multichannel wavelength division-multiplexing (WDM) [1], optical communication [2], linear and nonlinear spectroscopic applications [3–6], to laser based metrology [7]. It is desirable to combine high precision and simplicity with small size and the option of integration.

State-of-the-art wavemeters, such as double-folded Michelson interferometers [8], can readily provide a high spectral resolution of better than 10^{-6} . However, this comes at the cost of a fairly large instrument size (in the order of 10^6 wavelengths, i.e., typically a meter).

There are also simplified wavemeters which are suitable for miniaturization. Their working principle is based on two (or several) channels in which the transmission vs. wavelength is different [9]. If the mapping between the transmission of the channels and the wavelength is bijective (i.e., the transmission curve of each channel is strictly increasing or decreasing), the

normalized transmission ratio of the channels can be calibrated in the form of a look-up table (LUT). Miniaturization can be achieved by using the transmission functions of integrated optical wavelength filters [10], such as thin-film interference filters, photonic crystal waveguides [11], or multimode interference couplers [12]. This also allows the laser and its wavelength monitor to be integrated into a single device [13]. However, the operational range is confined to the region where the spectral sensitivities of all channels are either strictly increasing or decreasing.

In this paper, we present a new method for wavelength and power estimation, based on the calibrated transmission spectra of a micro-ring resonator (MRR), providing high precision and extended measurement range suitable for integrated optics. A wavemeter was constructed in an integrated optical design for verification of the method, which simply consists of a single, on-chip tunable MRR as an optical transmission filter and a single photodiode. The MRR used here is fabricated from $\text{Si}_3\text{N}_4/\text{SiO}_2$ with a box-shaped waveguide cross section (TriPleXTM) [14]. The wavelength and power of the incident light is estimated by analyzing the photodiode signals with neural networks and a nonlinear optimization algorithm.

The contribution of our work lies in the method for high-precision, range-extended wavelength and power estimation, which simplifies the optical requirements for design, fabrication and integration of the devices. Furthermore, with the proposed algorithm to estimate the wavelength, the spectral sensitivity of the MRR is not necessarily required to be strictly increasing or decreasing in the operational range. Therefore, the operational range is extended and more tunings can be applied for wavelength estimate (i.e., more heating voltages can be applied to the heater of the MRR), which results in a higher precision in the measurement. An advantage of this wavelength estimation method is that monotonicity is not required, allowing one to consider a larger number of physical implementations, including devices with randomly varying transmission. Thus, one may consider the transmission spectrum of a powder [15], or a multi-mode fiber [16], for example, as long as the transmission function is reproducible.

2. Principle of wavelength and power estimation

Fig. 1 shows the schematic of the wavemeter. Laser light with an unknown wavelength λ_x and unknown power P_x passes through a tunable optical filter. The transmission of the filter vs. wavelength, $f(\lambda, v_k)$, can be modified with an external control parameter, v_k . In our case, the filter is a single MRR equipped with an electric heater (see Fig.2). The control parameter is the voltage applied to the heater, which tunes the optical resonator length of the MRR and thereby modifies its transmission function. To estimate the wavelength of the input light field, a number of N different voltages are applied, where we define v_k as the k^{th} voltage. The transmitted light illuminates a photodiode, which yields a set of measurement signals y_k , in our case voltages. The sensitivity of the photodiode is denoted as $d(\lambda)$, which is a function of the wavelength λ . The measurement signal y_k is given by the product of the incident laser power, the transmission of the MRR, and the sensitivity of the photodiode. When including measurement noise, η_k , the measurement signal can be expressed as

$$y_k = P_x f(\lambda_x, v_k) d(\lambda_x) + \eta_k = P_x S(\lambda_x, v_k) + \eta_k. \quad (1)$$

Here we have abbreviated the product of the MRR transmission and photodiode sensitivity as the combined spectral sensitivity function $S(\lambda_x, v_k) = f(\lambda_x, v_k) d(\lambda_x)$.

To obtain the unknown wavelength, λ_x , and power, P_x , of incident light from measurements of y_k , we proceed in two steps:

1. Device calibration

The first step is to obtain information on the spectral sensitivity function. In principle,

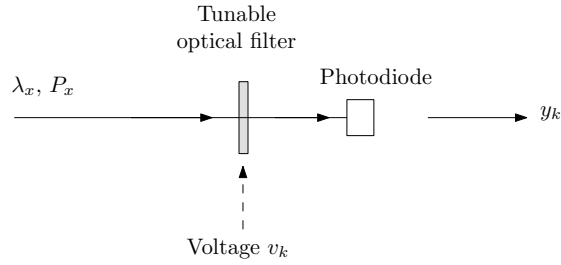


Fig. 1. General scheme of the wavemeter. Laser light with wavelength λ_x and power P_x passes the tunable color filter, i.e., a micro-ring resonator (MRR) in this paper. The spectral transmission function of the MRR can be changed by applying a heater voltage v_k . The transmitted light is collected by a photodiode, which yields a measurement signal y_k .

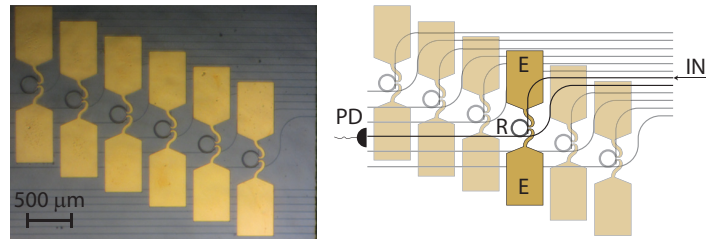


Fig. 2. Microscope picture of the waveguide chip (left) with micro-ring resonators (MRRs) and a schematic drawing (right) of the same chip. "R" denotes the MRR with the heater on top (gray). "E" denotes electrical contacts (gold colored) and the black lines represent waveguides. The fiber from the tunable laser was connected to the MRR from "IN". "PD" denotes the position of the photodiode. Since only one MRR was used at the same time, there was no crosstalk between the MRR and the heaters of neighboring MRRs.

$S(\lambda, v)$ may be derived via physical modeling of the MRR transmission and the photodiode response. However, in practice, the highest accuracy is achieved via calibration. Calibration requires injecting light at a known power at a number of known input wavelengths, λ , into the MRR. For each wavelength, λ , the heating voltage, v_k , of the MRR is tuned to N values, i.e., $k = 1, \dots, N$ with N the number of tunings; and the corresponding photodiode signals, y_k , ($k = 1, \dots, N$) are recorded for each pair of λ and v_k .

Fig. 3 shows typical sets of photodiode measurement data. Each data set is recorded at a different heater voltage v_k . An approximation for $S(\lambda, v)$ can then be obtained by fitting an analytical function to the data [17], such as a polynomial, a spline or a neural network (NN). A 2-layer neural network is able to model a broad range of nonlinearities [18–20] and, from a practical point of view, can be implemented and trained very conveniently, e.g., with a neural network toolbox [21]. Therefore a 2-layer neural network with Q neurons in the first layer and one in the second layer was chosen for our work. At a certain control voltage v_k , the output $y_k(\lambda)$ of the neural network is given as

$$y_k(\lambda) = P \cdot \hat{S}(\lambda, v_k) = P \sum_{i=1}^Q w_{1ik} \tanh(w_{2ik} \lambda + s_{1ik}) + s_{2ik}. \quad (2)$$

Eq. (2) models the spectral sensitivity curve as a superposition of step response functions (neurons), in this case chosen as tangent hyperbolic functions. w_{1ik} and w_{2ik} are the input

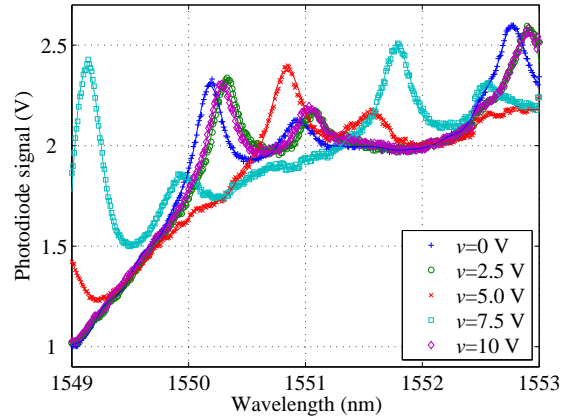


Fig. 3. Spectral sensitivity function $S(\lambda, \nu)$ at different ν . "+" : calibration data; lines: curves fitted by neural networks. For clarity, curves are shown only for five heating voltages $\nu=0$ V, 2.5 V, 5.0 V, 7.5 V and 10 V.

and output weights of the neural network, respectively; s_{1ik} and s_{2ik} are biases on the input and output neurons, respectively. To obtain a good compromise between a best fit and a minimum number of fit parameters, the number of neurons, Q , should be selected according to the required fitting accuracy of the neural network [20, 21].

2. Wavelength and power estimation

In the second step, light with an unknown wavelength, λ_x , and power, P_x , is sent into to the wavemeter. A set of N photodiode signals, y_k , is recorded via applying N different heater voltages, ν_k ($k = 1, \dots, N$). The heater voltages can be equally spaced (as in the experiments described in this paper), randomly selected or designed by the user beforehand. For each heater voltage, ν_k , a nonlinear equation, as described in Eq. (1) can be formed. By stacking N equations, a set of nonlinear equations is obtained as

$$Y \equiv \begin{bmatrix} y_1 \\ y_2 \\ \vdots \\ y_N \end{bmatrix} = \begin{bmatrix} P_x S(\lambda_x, \nu_1) + \eta_1 \\ P_x S(\lambda_x, \nu_2) + \eta_2 \\ \vdots \\ P_x S(\lambda_x, \nu_N) + \eta_N \end{bmatrix}. \quad (3)$$

The unknown wavelength, λ_x , and power, P_x , can be estimated by solving Eq. (3). Obtaining an analytical solution of Eq.(3) may be infeasible in practice. Alternatively, a numerical solution can be obtained by solving a nonlinear least squares (NLLS) problem as

$$(\hat{\lambda}_x, \hat{P}_x) = \arg \min_{\lambda_x, P_x} \underbrace{\frac{1}{N} |Y - \hat{Y}|^2}_J, \quad (4)$$

with Y defined in Eq. (3) and \hat{Y} defined as

$$\hat{Y} \equiv \begin{bmatrix} \hat{y}_1 \\ \hat{y}_2 \\ \vdots \\ \hat{y}_N \end{bmatrix} = \begin{bmatrix} \hat{P}_x \hat{S}(\hat{\lambda}_x, v_1) \\ \hat{P}_x \hat{S}(\hat{\lambda}_x, v_2) \\ \vdots \\ \hat{P}_x \hat{S}(\hat{\lambda}_x, v_N) \end{bmatrix}. \quad (5)$$

Here $\hat{S}(\lambda, v_k)$ is the approximated spectral sensitivity function that was obtained by calibration in Step 1. The mean-square-error between the measurement vector Y and the approximation \hat{Y} at certain guesses, $\hat{\lambda}_x$ and \hat{P}_x , is defined as the cost function $J = \frac{1}{N} |Y - \hat{Y}|^2$. Eq. (4) aims to find an appropriate $\hat{\lambda}_x$ and \hat{P}_x such that the approximation \hat{Y} is as close as possible to the measurement Y , i.e., J is minimized. In this way, the unknown wavelength, λ_x and power P_x , of the incident light field are estimated, i.e., the wavelength readout is obtained. By accurately approximating the spectral sensitivity, $S(\lambda, v_k)$, and increasing the number of tunings (i.e., more equations are used), the accuracy of $\hat{\lambda}_x$ and \hat{P}_x can be improved.

The special feature of our method is that the spectral sensitivity function, $\hat{S}(\lambda, v_k)$, is not necessarily bijective (i.e., strictly increasing or decreasing) with respect to wavelength, λ , in the operational range, as compared with the LUT method. Because of this, not only is the operational range of our wavemeter extended (non-monotonous regions are also allowed), but also the accuracy of the estimates is improved. Since monotonicity is not required, sensitivity curves with local peaks and troughs (and even multi-peaked and multi-troughed sensitivity functions) can be used for wavelength estimate. As more equations are added in Eq. (5), the accuracy of the estimate improves.

3. Experiments and results

Although our wavelength estimation method is not limited to one specific tunable optical filter, for an experimental demonstration, we used an available MRR. It consists of single-mode waveguide with a designed waveguide width of 450 nm. The waveguide chip is covered with a top cladding of 12 μm , upon which the heaters and electrodes are deposited. The cross section of the waveguide is box-shaped. The waveguide fabrication process is described in [14]. The radius of the MRR is $R=85.47 \mu\text{m}$ and the group index is $n_g=1.73$. The coupling gap between the straight waveguide and the MRR is about 1.1 μm , resulting in a power coupling coefficient of about 0.26. This corresponds to a free spectral range of about 2.6 nm and a Q -factor of about 6000. The through port of the MRR is connected to an independently calibrated, fiber-coupled tunable laser source (HP81689A, Agilent). The light transmitted through the MRR is coupled directly to a photodiode (FGA10, Thorlabs). The signal of the photodiode (i.e., y_k) is amplified and recorded by a computer via a data acquisition card (PCIe-6251, National Instruments). The heater voltage v_k is provided by the computer and a power amplifier.

To calibrate the sensitivity function, $S(\lambda, v)$, and to test the wavelength estimate method, two data sets were collected, denoted as $\{\lambda, v, y_c\}$ and $\{\lambda, v, y_t\}$, respectively. These two data sets were generated using a set of known wavelengths and heater voltages. The laser was tuned over the wavelength range from 1549 nm to 1553 nm, in 400 equal steps of 0.01 nm. The power was constant at 2 mW. For each wavelength, $N = 21$ heater voltages were applied, from 0 V to 10 V in steps of 0.5 V, and the corresponding photodiode signals were collected twice, one for calibration (i.e., y_c) and the other for test (i.e., y_t). Thus, in total, $401 \times 21 = 8421$ data points were recorded for calibration and the other 8421 data points for testing.

The settling time of the photodiode signal is about 0.5 milliseconds in case of a step heating voltage input. During data collection, the original sampling rate of the data acquisition card

is 1 kHz. To reduce the noise in the photodiode signal, 100 original samples are averaged to generate one data point. Readout takes about 0.04 seconds. Therefore getting one data point takes about 0.14 seconds. Because the communication between the control computer and the tunable laser and the tuning of the laser wavelength both take seconds, a typical time required for collecting both the calibration and test data sets is about two hours.

It can be seen in Fig. 3, that $S(\lambda, v_k)$ consists of a broad range of nonlinear variations vs. wavelength, resembling a set of mutually shifted Fabry-Perot resonator transmission functions. At longer wavelengths, the depth of the modulation decreases. This can be attributed to the overall heating of the optical waveguide chip, which causes the alignment between the optical filter and the waveguide to change over the course of the measurements.

During calibration, each sensitivity function at a particular voltage as a function of wavelength is approximated by a neural network, i.e., 21 neuronal network fits are performed, one for each heater voltage. To select an appropriate number of neurons, Q , in the network as presented by Eq. (2) (2 layers, with Q neurons in the first layer and one neuron in the second layer), the *variance accounted for* (VAF) was used as a criterion [22]. The VAF is defined by

$$A(\hat{y}_k, y_k) = \left(1 - \frac{\text{var}(\hat{y}_k - y_k)}{\text{var}(y_k)} \right) \times 100\%. \quad (6)$$

Here, $A(\hat{y}_k, y_k)$ is the VAF between \hat{y}_k and y_k , ranging from $-\infty$ to 100%. $\text{var}(y_k)$ is the variance of y_k . Fig. 4 shows the VAF of neural networks with respect to Q . As more neurons are used, the accuracy of the neural network increases until $Q = 14$. For $Q > 14$, the fitting accuracy is limited by the measurement noise in the data. Accordingly we decided to use 14 neurons in our network. The corresponding VAF (averaged over all 21 neural networks) is 99.63%, indicating an accurate approximation of the spectral sensitivity functions. This can be seen in Fig. 3, which shows an excellent agreement between the neural network fitting functions and the experimental data.

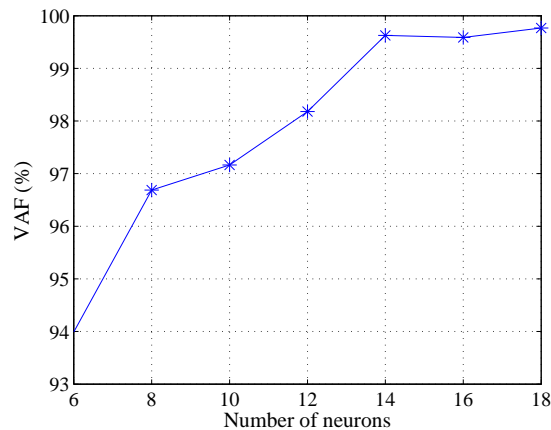


Fig. 4. Variance accounted for (VAF) of the neural networks with respect to the number of neurons (Q). The VAF in the vertical axis is averaged over VAF of all 21 neural networks. As more neurons are used, the accuracy of the neural network increases until $Q = 14$.

After calibration, the wavelength and power estimate algorithm was tested with the data set $\{\lambda, v, y_t\}$, where λ is considered unknown. For each "unknown" wavelength $\lambda_{x,i}$, $i \in [1, 401]$, the corresponding photodiode signals $y_{t,i,k}$, $k = 1, \dots, 21$ are scaled by a random number $p_{x,i} \in [0.1, 10]$. This simulates an input that has both an unknown wavelength and an unknown power,

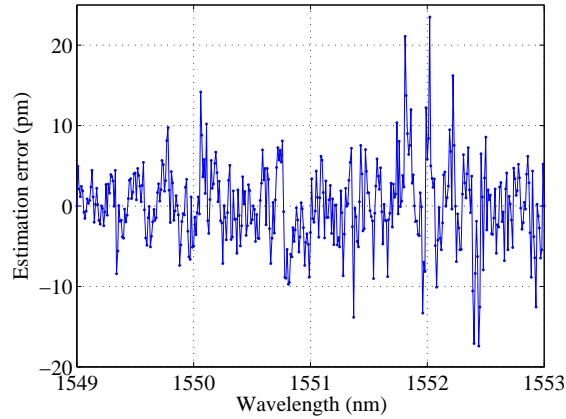


Fig. 5. Wavelength estimation error $\hat{\lambda}_x - \lambda_x$ in the test set.

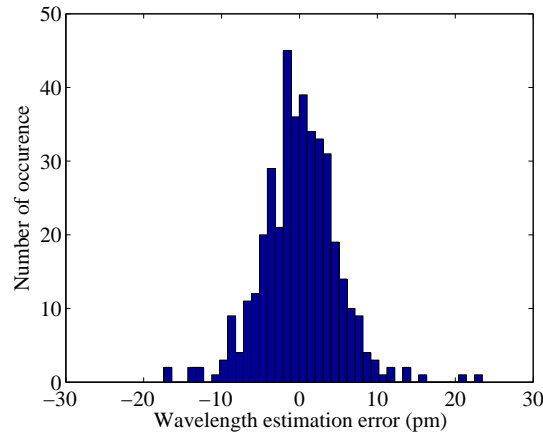


Fig. 6. Histogram of the wavelength estimation error. The maximal estimation error for the test set is 22 pm. 95% of the wavelength estimation errors are below 8 pm in the range between 1549 nm and 1553 nm.

which are to be estimated. The set of scaled photodiode signals are given as $\tilde{y}_{t,i,k} = p_{x,i}y_{t,i,k}$, $k = 1, \dots, 21$. Heating voltages, v_k , and signals, $\tilde{y}_{t,i,k}$, were then fed into the wavelength estimation algorithm and the unknown wavelength $\lambda_{x,i}$, and power-scaling factor $p_{x,i}$ were estimated.

Fig. 5 shows the wavelength estimation error $\hat{\lambda}_x - \lambda_x$ with respect to wavelength, λ_x , and Fig. 6 shows the estimation error in a histogram of occurrence. It can be seen that the maximum absolute wavelength estimation error for the test set is 22 pm and that 95% of the wavelength estimation errors are below 8 pm in the range from 1549 nm to 1553 nm. Fig. 7 shows the histogram of the relative power estimation error $(\hat{p}_x - p_x)/p_x$ with \hat{p}_x the estimate of p_x . The error in power estimation is 1.6% at maximum with respect to the known value; and in 95% cases, the power estimation error is less than 0.8% with respect to the known value.

To analyze whether the proposed neural network and nonlinear least square (NN+NLLS) method provides improved accuracy over a simple LUT method, we chose a LUT where the ratio between two spectral sensitivity curves strictly decreases. For the MRR used here, we

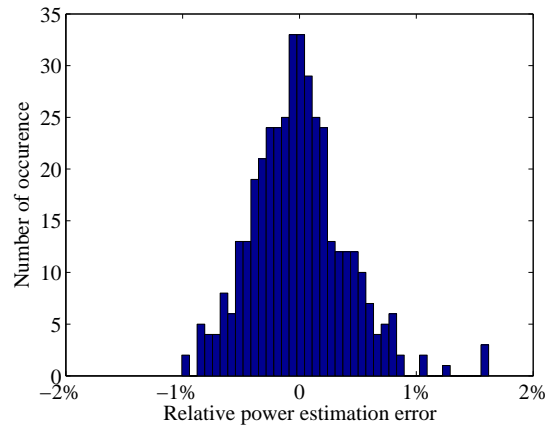


Fig. 7. Histogram of the relative power estimation error $(\hat{p}_x - p_x)/p_x$ in the test data set. The relative power estimation error is at maximum 1.6%, and in 95% of the cases less than 0.8%.

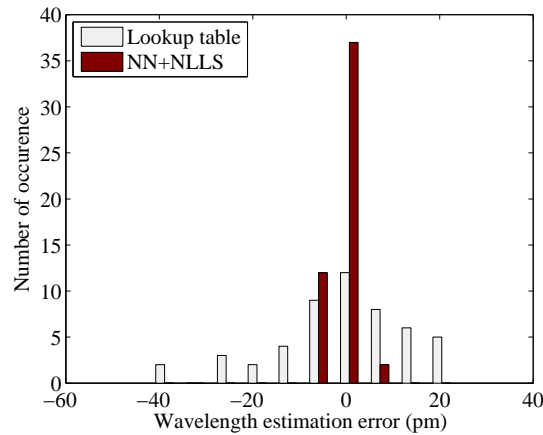


Fig. 8. Comparison between LUT and the proposed NN+NLLS method. 95% of the errors fall below 27 pm for LUT and 5 pm for the proposed method (about one fifth of that for LUT).

found a spectral region that satisfied this constraint, e.g., between 1550.3 nm and 1550.8 nm for the heater voltages $v_k=0$ V and 5 V. The wavelength was estimated using the LUT method and for the same data using the NN+NLLS method, as described above. The methods are compared in Fig. 8. The maximum wavelength estimation error in the named range is 42 pm for the LUT and 6 pm for our NN+NLLS approach. 95% of the errors are less than 27 pm for the LUT and less than 5 pm for NN+NLLS. This shows the NN+NLLS method, indeed, provides improved accuracy over that of LUT. The latter corresponds to a relative precision of about $3 \cdot 10^{-6}$. The improvement is as big as a factor of five.

4. Discussion

The accuracy of the wavelength and power estimation depends on not only on the accuracy of the neural networks, but also on the number of data points used for estimation and the noise in the data.

As more data points are used, more equations can be added to the nonlinear equation set and the accuracy of wavelength and power estimation will be improved. To verify this, wavelength and power estimation has been carried out where the number of data points used increases from 3 to 21 at a step of 2 (i.e., $N=3, 5, \dots, 21$). The result is shown in Fig. 9. It can be seen that the mean of the wavelength estimation error decreases as more data points are used as expected. There is a significant drop in the estimation error when more than 15 data points are used and the mean of the wavelength estimation error is limited to around 4 pm, which is mainly due to the modeling error of the neural networks and the noise in the measurement.

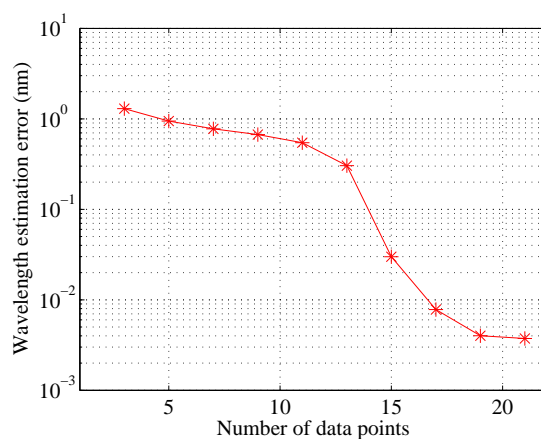


Fig. 9. Mean of the wavelength estimation error decreases as more data points are used in the estimation.

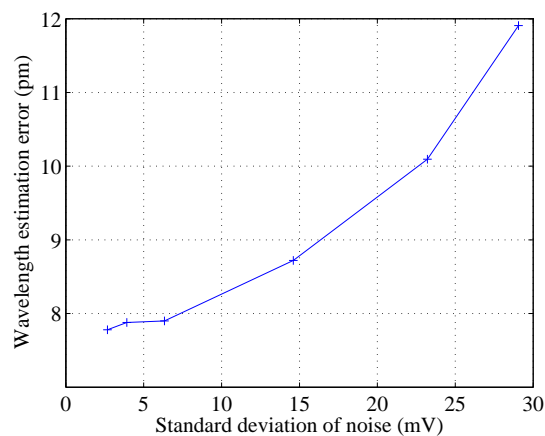


Fig. 10. Influence of noise on the wavelength estimation error. 95% of the wavelength estimation error is still within 10 pm when the standard deviation of the noise is 22.5 mV

Currently, the noise between the calibration and test data points has a mean value of 0.054 mV and standard deviation of 2.7 mV. To show how our algorithm is sensitive to the noise, a simulation has been carried out, where random noise has been added to the test data artificially and the wavelength and power are estimated. Simulation result has been shown in Fig. 10, which indicates that 95% of the wavelength estimation error is still within 10 pm when the standard deviation of the noise is 22.5 mV.

5. Conclusions

In conclusion, we have presented a novel method to measure the unknown power and wavelength of a laser with high precision and an extended measurement range. The method has been verified in a simple setup, based on an integrated optics micro ring resonator, which allows the wavemeter to be integrated with other on-chip optical components. Neural networks were used to approximate the spectral sensitivity functions of the optical channel at different heating voltages. When injecting light with an unknown wavelength and power, nonlinear equations are formed and solved to provide an estimate of the wavelength and power. In our experimental verification, we demonstrated a spectral precision of about 8 pm ($5 \cdot 10^{-6}$) in the wavelength range between 1549 nm and 1553 nm. A higher precision of 5 pm ($3 \cdot 10^{-6}$) was achieved in the range between 1550.3 nm and 1550.8 nm, which is a factor of five compared to a simple lookup of data.

The advantage of our approach is that it does not attempt to obtain a high precision and an increased wavelength range with a sophisticated and highly precise design of an appropriate spectral response function. Instead, our approach is able to handle all deviations that may enter via fabrication processes or fiber input and output coupling, as long as the optical transmission function is reproducible. Essentially, the approach replaces the need for a complex and precise optical design with a smart readout ("trading hardware for software"). This can help to reduce the cost of fabrication and expand the range of applications.

6. Acknowledgement

This work is supported by the STW project Smart Optical Systems: Waveguide Based External Cavity Semiconductor Laser Arrays (project NO. 10442) and in part by the Program for Zhejiang Leading Team of S&T Innovation (project NO. 2010R50036).